Speed Observer Structure of Induction Machine Based on Sliding Super-Twisting and Backstepping Techniques

Marcin Morawiec and Arkadiusz Lewicki

***Abstract*—This article presents an analysis of the two speed observer structures which are based on the backstepping and sliding super twisting approach. The observer stabilizing functions result from the Lyapunov theorem. To obtain the observer tuning gains the observer structure is linearized near the equilibrium point. The rotor angular speed is obtained from nonadaptive dependence. In the sensorless control system structure the classical PI controllers and transformation to the multiscalar variables are applied. The theoretical derivations are verified in experimental waveforms. Comparison of both speed observer structures is presented for nominal speed, load torque injections while regenerating mode, very low speed range and the uncertainties of nominal parameters of induction machine.**

***Index Terms*—Induction motor drives, observer, variable speed drives.**

I. Introduction

THE INDUCTION machine (IM) is a popular motor used in all industrial applications, especially for electric drive systems, to drive pumps, in transportation (train and trams) and in electromobility (electric or hybrid vehicles), in floating vessel [35]. The popularity of these machines is associated with a lower cost than permanent magnets machines and highly mechanical and thermal robust [1]. In transportation or in electromobility a speed sensor is necessary for safety reasons but in these applications redundancy can be guaranteed by a sensorless option (what is safer than only using the speed sensor which can be demaged). The name "sensorless" means a system without rotor electrical speed measurements. In addition to the rotor speed, the rotor flux vector components should be reconstructed. The rotor speed can be measured by a sensor (an encoder), but there is a risk associated with the loss of reliability of the control system structure which influences the whole electric drive system stability (sensitivity to vibrations, limited high-speed performance, installation issues, or measurements disturbances). In the sensorless control structure, an observer that reconstructed the rotor flux vector components as well as stator current vector components is typically used. The state variables of the observer can be estimated in (dq) reference frame as well as in $(\alpha\beta)$ stationary reference frame. The sensorless methods can be categorized into two groups. First one is based on high frequency injection [2]–[6] and the second one on techniques based on the mathematical model of the IM [7]–[30]. The approach based on the mathematical model of IM is popular but often a problem appears when the parameters of the IM are detuned or uncertain. Therefore, in the literature, in addition to classic solutions such as: nonlinear full order observers [7], [8], extended Luenberger observers [8], extended Kalman filters [9], model reference adaptive system (MRAS) [11], [12], there exists the methods of observers or controls named "robust." The group of robust estimators includes: based on backstepping approach [13], [14], adaptive [15], model predictive [16] the interconnected observers [17], [18] and above all based on the sliding-mode techniques [18]–[24]. The interconnected observer is rather complicated to introduce to industrial applications [16], [17], however, it gives good sensorless control performance, especially at low rotor speed range [17]. Sliding-mode approach has attractive advantages, such as fast response characteristics and robustness to disturbance. The satisfactory properties of the sensorless control are achieved in [20] in which the first-order sliding-mode (FOSM) was implemented but with the observer-backstepping technique. Due to the structure of FOSM the chattering has occurred. Therefore, in many applications it is better to use the high-order sliding mode (HOSM) [22]–[24], by which the chattering effect can be minimized. HOSMs presented in literature can be divided into a few groups: exact differentiation via sliding mode technique [25] which was named supertwisting algorithm (STA) and applied to observation in [26] and to estimations of state variables of IM [17], [22], [27] the homogeneous differentiators presented in [27]–[28].

The backstepping based speed observer were presented for example in [13] and [14]. Despite the use of the robust approach, the problem of reproducing observer state variables at low speeds has not been solved. The structure proposed in [13] works stable near to zero rotor speed but for the case of regenerating operation the properties of the speed observer are not sufficient. Behavior

Manuscript received January 2, 2020; accepted February 11, 2020. Date of publication May 29, 2020; date of current version November 18, 2020. This work was supported by National Science Centre of Poland under Grant 2018/31/N/ST7/03889. Paper no. TII-20-0017. *(Corresponding author: Marcin Morawiec.)*

Marcin Morawiec is with the Department of Electric Drives and Energy Conversion, Gdansk University of Technology, 80-233 Gdansk, Poland (e-mail: marcin.morawiec@pg.edu.pl).

Arkadiusz Lewicki is with the Department of Electric Drives and Energy Conversion, Gdansk University of Technology, 80-233 Gdansk, Poland (e-mail: arkadiusz.lewicki@pg.edu.pl).

Color versions of one or more of the figures in this article are available online at https://ieeexplore.ieee.org.

Digital Object Identifier 10.1109/TII.2020.2974507

of the others structure for example MRAS or adaptive full-order observer (AFO) in the regenerating mode are similar to [13]. The introduction of the appropriate modification presented in [31] to the AFO or MRAS structures makes them slightly more robust near to zero rotor speed operation and for regenerating modes. The better properties are achieved if the sliding-mode approach is included with the backsteppig approach what was noticed by Morawiec and Lewicki [20]. However, the sliding-mode approach is not necessary and it does not guarantee the stable work for the regenerating machine mode. In [20], the algebraic dependence from which the rotor speed is reconstructed was accordingly modified. As a result of proposed modification in [20], stable operation was achieved in the zero speed and the range of stable operation for the regenerating mode was increased. Proposed in [20] observer structure contains the large number of differential equations, tunning gains and is more complicated than the AFO speed observer structures [11], [15], [31], [32]. The main motivation of this article is to propose the speed observer structure of IM which has the simpler form than [20], [22]–[24] and better properties, especially in terms of the regenerating mode. The problems of stable work of a speed observer system at regenereting mode range and very low speed of machine were presented in many papers [17]–[20], [23]–[24], [31]–[32], [36]. In the sensorless control system and for the regenerating mode range close to zero speed (0.1 p.u. or smaller) the stator voltage amplitude and frequency is very small. As shown in [37], the IM can be unobservable (for the stator frequency equal to zero). Therefore, the two propositions of the speed observer are introduced. The first one is based on the backstepping technique and the second is based on the STA algorithm. Due to the structure of the speed observer the backstepping structure can be significantly simplified, what is shown in Section III. However, the backstepping approach itself does not cause that the speed observer will be robust on a disturbances. The proposed extension of the observer structure by the vector "*S*" gives possibilities of using the STA algorithm, which is much more resistant to observer structure disturbances (for example uncertainties of IM parameters, problems with the generating of very low stator voltage by a voltage source inverter at low speed range or unobservable working points of IM—the chattering effects due to sliding-mode can prevent it). Furthermore the rotor electric speed value can be obtained from the new algebraic equation in which the "robust term" is added. Comparison of properties of both structures with the new speed estimation manner will be presented for the same scenarios. Therefore, the main contribution of the article is to present the speed observer structure which is robust on the machine uncertainties of parameters, working stable at very low or zero rotor speed range, in regenerating mode and is "quite" simple to use in industrial applications.

II. Mathematical Model of IM

The differential equations of IM model, expressed in stationary reference frame ($\alpha\beta$) takes the following form [20], [22], [33]

$$\frac{d\boldsymbol{i}_s}{d\tau} = a_1(-R_s\boldsymbol{i}_s + \boldsymbol{u}_s) - a_2\frac{d\boldsymbol{\psi}_r}{d\tau} \tag{1}$$

$$\frac{d\boldsymbol{\psi}_r}{d\tau} = -a_3\boldsymbol{\psi}_r + j\omega_r\boldsymbol{\psi}_r + a_4\boldsymbol{i}_s \tag{2}$$

$$\frac{d\omega_r}{d\tau} = \frac{1}{J}(T_e - T_L) \tag{3}$$

where:

$\boldsymbol{i}_s$, $\boldsymbol{u}_s$, ψ_r are the current, voltage and the rotor flux vectors, respectively,

$$a_1 = \frac{L_r}{w_\sigma},\ a_2 = \frac{L_m}{w_\sigma},\ a_3 = \frac{R_r}{L_r},\ a_4 = \frac{R_rL_m}{L_r}. \tag{4}$$

The following assumptions are taken into account: the IM parameters (4) are known and constant, the stator current vector components $i_{s\alpha}$, $i_{s\beta}$ can be measured, the stator voltage vector components $u_{s\alpha}$, $u_{s\beta}$ are the control variables, rotor flux vector components $\psi_{r\alpha}$, $\psi_{r\beta}$ as well as $i_{s\alpha}$, $i_{s\beta}$ and the rotor angular speed ω_r are estimated by the speed observer structure.

In further considerations, vector $\boldsymbol{S}$ will be taken into account, defined as follows:

$$\boldsymbol{S} = -a_3\boldsymbol{\psi}_r + j\omega_r\boldsymbol{\psi}_r + a_4\boldsymbol{i}_s. \tag{5}$$

Operation domain *D* is defined as follows:

$\boldsymbol{\psi}_r^{\max}$, $\boldsymbol{i}_s^{\max}$, $\boldsymbol{\omega}_r^{\max}$, $\boldsymbol{T}_L^{\max}$ are, respectively, the maximum values of the rotor flux vector, stator current vector, rotor speed, and load torque such that $|\boldsymbol{\psi}_r| \le \boldsymbol{\psi}_r^{\max}$, $|\boldsymbol{i}_s| \le \boldsymbol{i}_s^{\max}$, $|\boldsymbol{\omega}_r| \le \boldsymbol{\omega}_r^{\max}$, $|\boldsymbol{T}_L| \le \boldsymbol{T}_L^{\max}$ ($\boldsymbol{T}_L^{\max} = 0.745$ p.u. for $\boldsymbol{i}_s^{\max} = 1.1$ p.u.).

III. Speed Observer of IM Extended to Integrators

The approach which is based on the augmentation of a system by an integrator has been named in [29] (Lemma 2.8) *integrator backstepping*. According to this lemma the system $\dot{x} = f(x) + g(x)u$ can be augmented to integrator

$$\dot{x} = f(x) + g(x)\xi \tag{6}$$

$$\dot{\xi} = u \tag{7}$$

and there exists the continuous and differentiable control law $u = \alpha(x)$ which can be treat as the virtual control and the tracking error $z = \xi - \alpha(x)$. There is a smooth function, positively defined and radially unbounded $V(x, \xi, z)$ such that

$$\dot{V}(x, \xi, z) \le -W(x, \xi, z) \le 0 \tag{8}$$

where $W(x, \xi, z) > 0$ is positive define in $z = \xi - \alpha(x)$ and guarantees the global boundedness of state variables as well as convergence of (x, ξ, z) to zero in finite time (or to the largest invariant set as it was presented in [29]). The backstepping method presented above allows to extend the observer model of the IM to an integrator.

Authors of this article propose two different approaches to obtain the stabilization functions for the same observer structure. The observer model will be rewritten in stationary reference

frame ($\alpha\beta$). The differential equations of the proposed observer have the following form:

$$\frac{d\hat{i}_{s\alpha}}{d\tau} = a_1(-R_s i_{s\alpha} + u_{s\alpha}) - a_2\hat{S}_\alpha + v_\alpha \tag{9}$$

$$\frac{d\hat{i}_{s\beta}}{d\tau} = a_1(-R_s i_{s\beta} + u_{s\beta}) - a_2\hat{S}_\beta + v_\beta \tag{10}$$

$$\frac{d\hat{\psi}_{r\alpha}}{d\tau} = \hat{S}_\alpha + v_{\psi\alpha} \tag{11}$$

$$\frac{d\hat{\psi}_{r\beta}}{d\tau} = \hat{S}_\beta + v_{\psi\beta} \tag{12}$$

where on the left side of differential equations stabilizing function are included (marked by $v_{\alpha,\beta}$, $v_{\psi\alpha,\beta}$) and $i_{s\alpha,\beta}$, $u_{s\alpha,\beta}$ are known or measured.

The observer structure (9)–(12) is stable if the appropriate stabilizing functions will be determined. In order to stabilize structure (9)–(12) the following integrators structure should be considered:

$$\frac{d\hat{S}_\alpha}{d\tau} = -\hat{S}_\alpha(a_3+a_2a_4) - \omega_r\hat{S}_\beta + R_r a_2(-R_s i_{s\alpha} + u_{s\alpha}) + v_{S\alpha} \tag{13}$$

$$\frac{d\hat{S}_\beta}{d\tau} = -\hat{S}_\beta(a_3+a_2a_4) + \omega_r\hat{S}_\alpha + R_r a_2(-R_s i_{s\beta} + u_{s\beta}) + v_{S\beta} \tag{14}$$

where ω_r is marked as known value.

Taking into account (21)–(23), integrators structure (5), (13), and (14), the tracking errors of the state variables of the proposed observer (9)–(12) have the form

$$\frac{d\tilde{i}_{s\alpha}}{d\tau} = -a_2\tilde{S}_\alpha + v_\alpha \tag{15}$$

$$\frac{d\tilde{i}_{s\beta}}{d\tau} = -a_2\tilde{S}_\beta + v_\beta \tag{16}$$

$$\frac{d\tilde{\psi}_{r\alpha}}{d\tau} = \tilde{S}_\alpha + v_{\psi\alpha} \tag{17}$$

$$\frac{d\tilde{\psi}_{r\beta}}{d\tau} = \tilde{S}_\beta + v_{\psi\beta} \tag{18}$$

$$\frac{d\tilde{S}_\alpha}{d\tau} = -\tilde{S}_\alpha(a_3 + a_2a_4) - \omega_r\tilde{S}_\beta + v_{S\alpha} \tag{19}$$

$$\frac{d\tilde{S}_\beta}{d\tau} = -\tilde{S}_\beta(a_3 + a_2a_4) + \omega_r\tilde{S}_\alpha + v_{S\beta} \tag{20}$$

where

$$\tilde{i}_{s\alpha} = \hat{i}_{s\alpha} - i_{s\alpha},\ \tilde{i}_{s\beta} = \hat{i}_{s\beta} - i_{s\beta}, \tag{21}$$

$$\text{and } \tilde{\psi}_{r\alpha} = \hat{\psi}_{r\alpha} - \psi_{r\alpha},\ \tilde{\psi}_{r\beta} = \hat{\psi}_{r\beta} - \psi_{r\beta} \tag{22}$$

$$\tilde{S}_\alpha = \hat{S}_\alpha - S_\alpha,\ \tilde{S}_\beta = \hat{S}_\beta - S_\beta. \tag{23}$$

On the other hand, it is possible to extend the observer structure (9)–(12) (taking into account the integrator backstepping lemma) to the integrators with errors dynamic

$$\frac{d\tilde{S}_\alpha}{d\tau} = \tilde{i}_{s\alpha} \tag{24}$$

$$\frac{d\tilde{S}_\beta}{d\tau} = \tilde{i}_{s\beta}. \tag{25}$$

Comparing (19), (20) to (24), (25) one obtains

$$v_{S\alpha} = \tilde{i}_{s\alpha} + k_s(\tilde{S}_\alpha(a_3 + a_2a_4) + \omega_r\tilde{S}_\beta) \tag{26}$$

$$v_{S\beta} = \tilde{i}_{s\beta} + k_s(\tilde{S}_\beta(a_3 + a_2a_4) - \omega_r\tilde{S}_\alpha) \tag{27}$$

where $v_{S\alpha}$ and $v_{S\beta}$ are stabilizing functions the integrators structure (13), (14), and $k_s > 0$.

Using above comparison between integrators structures it is not necessary to apply the further backstepping procedure [29] [which significantly reduces the mathematical procedures and simplifies the observer structure—the observer structure does not need to be extended with an integrator (24), (25) because of the "*S*" vector differential equations and new obtained functions (26), (27)]. In the next step, the other stabilizing functions will be achieved by using the Lyapunov stability theorem.

The quadratic of Lyapunov function has the form

$$V_1 = 0.5\left(\tilde{i}_{s\alpha}^2 + \tilde{i}_{s\beta}^2 + \tilde{\psi}_{r\alpha}^2 + \tilde{\psi}_{r\beta}^2 + \tilde{S}_\alpha^2 + \tilde{S}_\beta^2\right). \tag{28}$$

The derivative of (28) with taking into account (15)–(20) and (26), (27), takes the form

$$\dot{V}_1 = \tilde{i}_{s\alpha}(-a_2\tilde{S}_\alpha + v_\alpha) + \tilde{i}_{s\beta}(-a_2\tilde{S}_\beta + v_\beta) + \tilde{\psi}_{r\alpha}(\tilde{S}_\alpha + v_{\psi\alpha}) + \tilde{\psi}_{r\beta}(\tilde{S}_\beta + v_{\psi\beta}) + \tilde{S}_\alpha(\tilde{i}_{s\alpha}) + \tilde{S}_\beta(\tilde{i}_{s\beta}) \le 0 \tag{29}$$

The observer structure is asymptotic stable if

$$v_\alpha = -c_s(1 - a_2)\tilde{S}_\alpha \tag{30}$$

$$v_\beta = -c_s(1 - a_2)\tilde{S}_\beta \tag{31}$$

$$v_{\psi\alpha} = -k_\psi\tilde{S}_\alpha \tag{32}$$

$$v_{\psi\beta} = -k_\psi\tilde{S}_\beta \tag{33}$$

and (26), (27), where $c_s, k_\psi > 0$.

Further considerations should demonstrate that for system (1), (2) the estimation errors of the proposed observer can exponentially converge to zero in finite time $t > t_1$ (under condition of no disturbances of the system). If to proposed observer structure (9)–(12) and (13), (14) the following uncertainties terms are introduced: $\Delta a_i \le \Delta a_i^{\max}$, $\Delta a_\psi \le \Delta a_\psi^{\max}$, and $\Delta a_S \le \Delta a_S^{\max}$ (where index max means the maximum value of an uncertainties coefficient). Since system (1), (2) stays in operation domain *D*, hence if

$$v_\alpha = \max\left\{-c_s(1 - a_2)\tilde{S}_\alpha - \Delta a_i\right\} + \delta_\alpha \tag{34}$$

$$v_\beta = \max\left\{-c_s(1 - a_2\tilde{S}_\beta) - \Delta a_i\right\} + \delta_\beta \tag{35}$$

$$v_{\psi\alpha} = \max\left\{-k_\psi\tilde{S}_\alpha - \Delta a_\psi\right\} + \delta_\psi \tag{36}$$

$$v_{\psi\beta} = \max\left\{-k_\psi\tilde{S}_\beta + \Delta a_\psi\right\} + \delta_\psi \tag{37}$$

$$v_{S\alpha} = \max\left\{\tilde{i}_{s\alpha} + k_s(\tilde{S}_\alpha(a_3 + a_2a_4) + \omega_r\tilde{S}_\beta - \Delta a_S)\right\} + \delta_S \tag{38}$$

$$v_{S\beta} = \max\left\{\tilde{i}_{s\beta} + k_s(\tilde{S}_\beta(a_3 + a_2a_4) - \omega_r\tilde{S}_\alpha - \Delta a_S)\right\} + \delta_S \tag{39}$$

with $\delta_\alpha, \delta_\beta, \delta_\psi, \delta_S > 0$ and for $\tilde{i}_{s\alpha,\beta} \le \varepsilon_1, \tilde{S}_{\alpha,\beta} \le \varepsilon_2, \tilde{\psi}_{r\alpha} \le \varepsilon_3$, $\varepsilon_{1,2,3} \ll 1$ are sufficient small reals, there is assumed $(c_s, k_\psi) \approx 1$, the derivative (29) has the following form:

$$\dot{V}_1 = -\delta_\alpha |i_{s\alpha}| - \delta_\beta |i_{s\beta}| - \delta_{\psi\alpha}\left|\tilde{\psi}_{r\alpha}\right| - \delta_{\psi\beta}\left|\tilde{\psi}_{r\beta}\right| \le -\mu\sqrt{V_1} \tag{40}$$

where $\mu = \min(\sqrt{2}\delta_\alpha, \sqrt{2}\delta_\beta, \sqrt{2}\delta_\psi, \sqrt{2}\delta_S)$ and value $k_s > 0$ can be determined from

$$k_s = \frac{\left|(\tilde{i}_{s\alpha}\tilde{S}_\alpha + \tilde{i}_{s\beta}\tilde{S}_\beta)\right|}{\left|(\tilde{S}_\alpha^2 + \tilde{S}_\beta^2)(a_3 + a_2a_4) - \Delta a_S^{\max}(\tilde{S}_\alpha + \tilde{S}_\beta)\right|}. \tag{41}$$

The condition (40) implies the convergence of vectors values $\hat{\boldsymbol{i}}_s$ to $\boldsymbol{i}_s$, $\hat{\boldsymbol{\psi}}_r$ to $\boldsymbol{\psi}_r$ and $\hat{\boldsymbol{S}}$ to $\boldsymbol{S}$ in finite time, noted as t_2.

Remark 1: The estimation errors (23) stabilized observer structure (9)–(12) should be determined as follows:

$$\tilde{S}_\alpha = \hat{S}_\alpha - \left(-a_3\hat{\psi}_{r\alpha} - \hat{\omega}_r\hat{\psi}_{r\beta} + a_4\hat{i}_{s\alpha}\right) \triangleq \hat{S}_\alpha - S_\alpha \tag{42}$$

$$\tilde{S}_\beta = \hat{S}_\beta - \left(-a_3\hat{\psi}_{r\beta} + \hat{\omega}_r\hat{\psi}_{r\alpha} + a_4\hat{i}_{s\beta}\right) \triangleq \hat{S}_\beta - S_\beta. \tag{43}$$

Remark 2: Speed of convergence of the proposed observer structure is depend on the tuning gains $c_s > 0$ and $0 < k_\psi \le 1$. It is easy to prove that for $k_\psi > 1$ the observer structure will be unstable, for example taking (17), (18), for $k_\psi = 2$, hence $\dot{\tilde{\psi}}_{r\alpha} = -\tilde{S}_\alpha$ and $\dot{\tilde{\psi}}_{r\beta} = -\tilde{S}_\beta$.

Remark 3: Value of estimated rotor speed results from vector $(\hat{\boldsymbol{S}} \times \hat{\boldsymbol{\psi}}_{\boldsymbol{r}})$ and scalar $(\hat{\boldsymbol{S}} \cdot \hat{\boldsymbol{\psi}}_{\boldsymbol{r}})$ multiple of vector $(\hat{\boldsymbol{S}}, \hat{\boldsymbol{\psi}}_{\boldsymbol{r}})$ and in the proposed integrators structure (13), (14) $\omega_r = \hat{\omega}_r$ estimated from the dependence

$$\hat{\omega}_r = \frac{\hat{S}_\beta\hat{\psi}_{r\alpha} - \hat{S}_\alpha\hat{\psi}_{r\beta} - a_4(\hat{i}_{s\beta}\hat{\psi}_{r\alpha} - \hat{i}_{s\alpha}\hat{\psi}_{r\beta}) + C_f(\hat{S}\cdot\hat{\psi}_r)}{\hat{\psi}_{r\alpha}^2 + \hat{\psi}_{r\beta}^2} \tag{44}$$

$$\begin{aligned}\left(\hat{\boldsymbol{S}}\cdot\hat{\boldsymbol{\psi}}_{\mathrm{r}}\right) &= \hat{S}_\alpha\hat{\psi}_{r\alpha} + \hat{S}_\beta\hat{\psi}_{r\beta} - a_4(\hat{i}_{s\alpha}\hat{\psi}_{r\alpha} + \hat{i}_{s\beta}\hat{\psi}_{r\beta}) \\ &\quad + a_3(\hat{\psi}_{r\alpha}^2 + \hat{\psi}_{r\beta}^2)\end{aligned} \tag{45}$$

where $\hat{\psi}_{r\alpha}^2 + \hat{\psi}_{r\beta}^2 \ne 0$ and

$$C_f = k_f \mathrm{sgn}\,(s_\omega) = \begin{cases} 1 & s_\omega < 0 \\ -1 & s_\omega \ge 0 \end{cases} \tag{46}$$

$s_\omega = (\hat{\mathbf{S}}\cdot\hat{\psi}_{\mathbf{r}})$ and $0 < k_f < 5$.

For the very low rotor speed $s_\omega = \omega_r^*$ where ω_r^* is the reference rotor speed (input to the control system).

Remark 4: Practical stability analysis presented in this section is satisfied for the nominal parameters of the IM and with an uncertainties terms introduced to observer structure. The stability analysis of observer-controller system has been presented in [17], [18], [20], and [23]. The proof of stability procedure may be carried out in a similar manner. Despite the fact that the analysis shows the convergence of the observer structure to zero, in practical applications in cases of many different disturbances, estimation errors take values close to zero. Influence parameters uncertainty on the sensorless control system will be demonstrated in the experimental tests.

Proposed speed observer structure (9)–(14) has no robust term (only dependence (44) contains switching term), therefore, in the Section V, the STA will be introduced.

IV. Tunnig Gains of Speed Observer

The observer gains influence the speed observer convergences. The tunning gains can be specified from the model of the observer errors (15)–(20) (nonlinear approach) or can be linearized near an equilibrium points. In the drive system the second one approach is more desirable than the first due to possibility of taking into account specifics machine working points in which it can be unstable. In order to examine the impact of the observer gains to stability range, the nonlinear observer system (15)–(20) is linearized near the equilibrium point. The linearized system has the general form

$$\frac{d}{dt}\Delta\mathbf{x}(t) = \mathbf{A}\Delta\mathbf{x}(t) + \mathbf{B}\Delta\mathbf{u}(t) \tag{47}$$

where $\mathbf{A}$ and $\mathbf{B}$ are the Jacobian matrices and $\Delta\mathrm{x}(t) = [\tilde{i}_{sd}, \tilde{i}_{sq}, \tilde{\psi}_{rd}, \tilde{\psi}_{rq}, \tilde{S}_d, \tilde{S}_q]^T$, $\Delta\mathrm{u}(t)$ is treated as known control inputs.

Taking into account the model of observer structure errors and its linearization near the equilibrium point, matrix $\mathbf{A}$ is defined as follows:

$$\mathbf{A} = \begin{bmatrix} 0 & c_{ss}\omega_\psi & 0 & 0 & a_5 & 0 \\ -c_{ss}\omega_\psi & 0 & 0 & 0 & 0 & a_5 \\ 0 & 0 & -k_\psi & k_{\psi\psi}\omega_\psi & k_{\psi\psi} & 0 \\ 0 & 0 & -k_{\psi\psi}\omega_\psi & -k_\psi & 0 & k_{\psi\psi} \\ 1 & 0 & 0 & 0 & -a_6 & a_7 \\ 0 & 1 & 0 & 0 & a_7 & -a_6 \end{bmatrix},$$

where

$$\begin{aligned} &c_{ss} = (1 - c_s), k_{\psi\psi} = (1 - k_\psi), a_5 = -a_2c_{ss} \\ &a_6 = (a_3 + a_2a_4)(1 - k_s), a_7 = (-\omega_r + \omega_\psi(1 - k_s)) \end{aligned}.$$

The estimator system is oriented with the rotor flux vector $\vec{\psi}_r$, so $\psi_{rd} = |\vec{\psi}_r|, \psi_{rq} = 0$ and the stator current vector components and ω_ψ can be treated as follows:

$$i_{sd} = \frac{\psi_{rd}^*}{L_m},\ i_{sq} = \frac{T_L^*}{a_4\psi_{rd}^*},\ \omega_\psi = a_2\left(\frac{i_{sq}}{\psi_{rd}^*} + \omega_r^*\right)$$

where $(*)$ means the values for equilibrium points.

The stability analysis for the proposed speed observer is presented in Fig. 1 and 2. In Fig. 1(a), the eigenvalues of the linearized observer system during the rotor speed changing from -1.0 to 1.0 p.u. are shown. In Fig. 1(b), the load torque was changed from -1.0 to 1.0 p.u., the rotor speed was 1.0 p.u. (for -T_L the IM worked in regenerating mode. For both these cases the speed observer was stable (for the constant observer gains). However in this analysis it was assumed ideal case in which the error of estimation of rotor speed error is equal to zero.

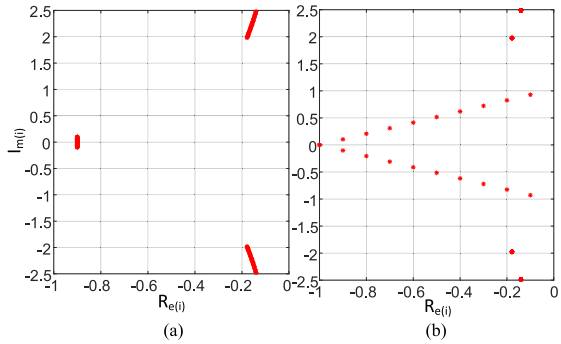

Fig. 1. Spectrum of matrix **A** of the linearized observer system for $c_s = 0.5$, $k_\psi = 1$, $k_s = 0.5$ while (a) the rotor speed is changing from -1.0 to 1.0 p.u. and (b) T_L is changing from -1.0 to 1.0 p.u., $\omega_r = 1.0$ p.u.

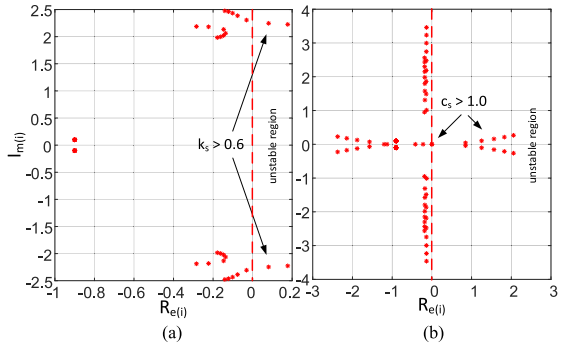

Fig. 2. Spectrum of matrix **A** of the linearized observer system for $c_s = 0.5$, $k_\psi = 0.9$, $\omega_r = 1.0$ p.u., $T_L = 0.9$ p.u. while (a) k_s is changing from 0.1 to 0.7 p.u. and (b) c_s is changing from 0.1 to 1.5.

In Fig. 2(a), the rotor speed was 1.0, $T_L = 0.9$ p.u., $c_s = 0.5$, $k_\psi = 0.9$ and k_s was changing from 0.1 to 0.7. For k_s higher than 0.5 the observer structure is unstable. In Fig. 2(b), c_s was changing from 0.1 to 1.5. If $c_s = 1.0$ then the observer structure is unstable.

From the location of eigenvalues of the linearized observer system (poles) presented in Fig. 1 and 2 it can conclude that c_s should be smaller than 1.0., $0 < k_\psi \leq 1$ and $0 < k_s \leq 0.5$ then the observer structure will be stable. Obtained observer tunning gains using theoretical analysis presented in this section were introduced to the simulations and in the experimental stand.

V. Speed Observer of IM Based on Sliding STA

In [25], a robust exact differentiator ensuring finite time convergence was designed, as an application of the STA [30]. This algorithm was named supertwisting. It is counted to a sliding HOSM and simple to apply in the sensorless control of a machine [17], [22], [24], [26], [28], [30]. The STA form dedicated to estimation can be written as

$$\begin{cases} \frac{d\hat{x}_1}{d\tau} = f(\hat{x}_2) + \lambda|\hat{x}_1 - x_1|^{0.5}\text{sgn}(\hat{x}_1 - x_1) + \Delta_1 \\ \frac{d\hat{x}_2}{d\tau} = \alpha\text{sgn}(\hat{x}_1 - x_1) + \Delta_2 \end{cases} \tag{48}$$

where α, λ are the switching gains and $\Delta_{1,2}$ represent the perturbation terms which can be $\Delta_{1,2} \approx 0$.

The conditions for the continuous STA-based observer to converge in finite time are presented and discussed in [26] and [28] and have the following form:

$$\begin{aligned} &\alpha \gg C \\ &\lambda^2 = 4C\tfrac{\alpha+C}{\alpha-C} \end{aligned} \tag{49}$$

where $C > 0$ is the Lipschitz's constant.

The earlier STA algorithm can be used in the observer structure (9)–(12) and the integrators (19), (20). The speed observer structure has the following form:

$$\frac{d\hat{i}_{s\alpha}}{d\tau} = a_1(-R_s i_{s\alpha} + u_{s\alpha}) - a_2\hat{S}_\alpha + \lambda\left|\tilde{i}_{s\alpha}\right|^{0.5}\text{sgn}(\tilde{i}_{s\alpha}) \tag{50}$$

$$\begin{aligned} \frac{d\hat{S}_\alpha}{d\tau} = &-\hat{S}_\alpha(a_3 + a_2a_4) - \hat{\omega}_r\hat{S}_\beta + R_r a_2(-R_s i_{s\alpha} + u_{s\alpha}) \\ &+ \alpha\text{sgn}(\tilde{i}_{s\alpha}) \end{aligned} \tag{51}$$

$$\frac{d\hat{i}_{s\beta}}{d\tau} = a_1(-R_s i_{s\beta} + u_{s\beta}) - a_2\hat{S}_\beta + \lambda\left|\tilde{i}_{s\beta}\right|^{0.5}\text{sgn}(\tilde{i}_{s\beta}) \tag{52}$$

$$\begin{aligned} \frac{d\hat{S}_\beta}{d\tau} = &-\hat{S}_\beta(a_3 + a_2a_4) + \hat{\omega}_r\hat{S}_\alpha + R_r a_2(-R_s i_{s\beta} + u_{s\beta}) \\ &+ \alpha\text{sgn}(\tilde{i}_{s\beta}) \end{aligned} \tag{53}$$

the rotor flux components can be obtained from (11), (12) taking into account (32), (33) and the rotor electric speed from (44).

Taking into account (49) and if $C = 0.005$, $\alpha = 0.2$ then $\lambda < 0.145$. In order to reduce the chattering in the experimental setup coefficient $\lambda = 0.035$ was taken. This approach is sufficient to obtain the stable work of the drive system with IM what will be presented in Section VI. However similar to [17], [20] and presented in Section III analysis can be applied to more precisely estimate value of the coefficient α and λ (using the practical stability analysis).

The (second-order) STA approach limits the chattering effects with comparison to the FOSM and it allows to achieve robust observer structure. This problem was developed and shown in [26], [27], and [34]. The HOSM sliding can practically eliminate the chattering (remove relative-degree restriction [34]). In the next section, the comparison of experimental tests of two proposed observer structures will be carried out.

VI. Experimental Results

The experimental tests were carried out on a 5.5 kW drive system supplied by the voltage source converter system. The motor drive system parameters are given in Table III. The control system was implemented in an interface with a DSP Sharc ADSP21363 floating point signal processor and Altera Cyclone 2 FPGA. The transistor switching frequency was 3.3 kHz but the sampling time was 150 μs. The stator current was measured by the current transducers LA 25-NP—in the phases "a" and "b" and transformed to the $(\alpha\beta)$ reference frame by using the Park transformation. The control system structure is presented in Fig. 3. There are a four classical proportional-integral (PI) controllers and the multi-scalar transformation of variables (see

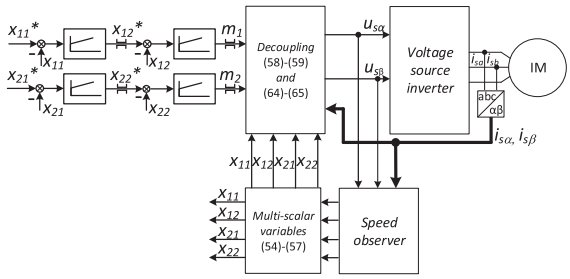

Fig. 3. Sensorless control structure with proposed speed observer and multiscalar variables (description in the Appendix).

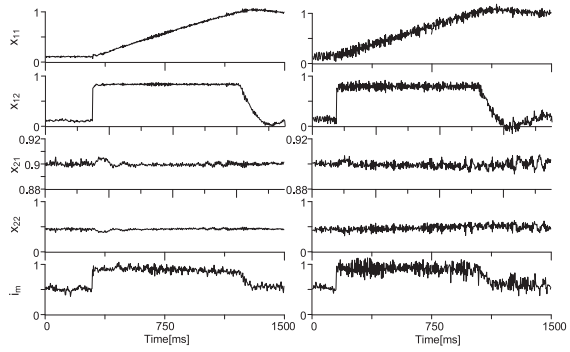

Fig. 4. Machine is starting up to 1.0 p.u. in case of (a) backstepping-based speed observer and (b) STA-based speed observer.

in Appendix). The control system structure is described by the mathematical dependences in the Appendix. In all tests the reference square of rotor flux was $x_{21}{}^{*} = 0.92$ p.u. and the value of load torque was limited to $T_{L\max} = 0.7$–0.8 p.u. The electromagnetic torque of IM is limited to 0.7–0.8 p.u. (in dynamic IM states due to a maximum value of inverter current equal to 1.2–1.35 p.u.). The following waveform of variables are shown as:

x_{11} —Estimated rotor angular speed.
$x_{12} = \hat{\psi}_{r\alpha}\hat{i}_{s\beta} - \hat{\psi}_{r\beta}\hat{i}_{s\alpha}$ —Variable proportional to electromagnetic torque.
$x_{21} = \hat{\psi}^2_{r\alpha} + \hat{\psi}^2_{r\beta}$ —Square of rotor flux vector.
$x_{22} = \hat{\psi}_{r\alpha}\hat{i}_{s\alpha} + \hat{\psi}_{r\beta}\hat{i}_{s\beta}$ —Additional variable.
i_m —Stator current vector module.
$\tilde{\omega}_r = \hat{\omega}_r - \omega_r$ —Estimated rotor speed error.

In order to show the properties of two different observer structures, in the control structure, the continuous PI controllers have been applied. The experimental tests have been divided into three scenarios:

1) Machine start-up to nominal speed, reverse and very low speed reverse (Section VI-A and Fig. 4–6).
2) Robustness against nominal parameters detuning (parameter uncertainties) (Section VI-B and Fig. 7–9).
3) Load torque injections for low rotor speed (Section VI-C and Fig. 10–12).

In order to compare both speed observer structures in will be always presented the waveforms for observer based on the backstepping stabilization functions (it is shown in Section III) and presents the waveforms for the STA approach.

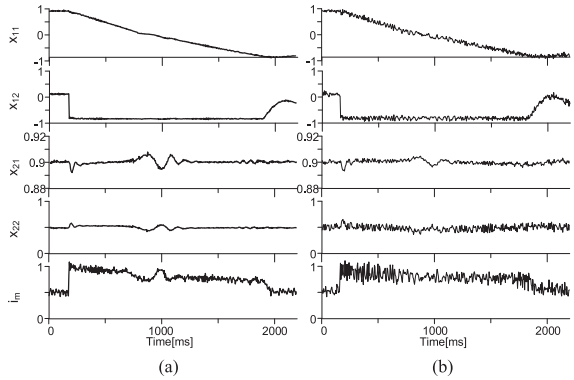

Fig. 5. Machine is reversing from 0.95 to −0.95 p.u. in case of (a) backstepping-based speed observer and (b) STA-based speed observer.

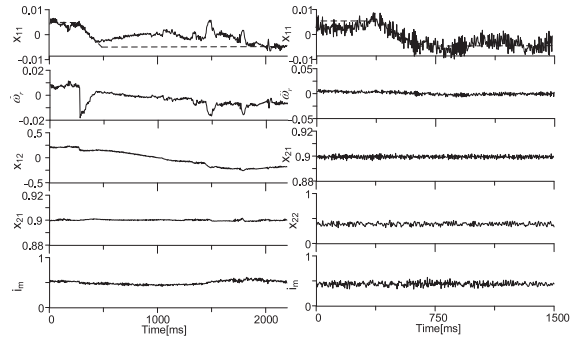

Fig. 6. Machine is reversing from 0.005 to −0.005 p.u. in case of (a) backstepping-based speed observer and (b) STA-based speed observer.

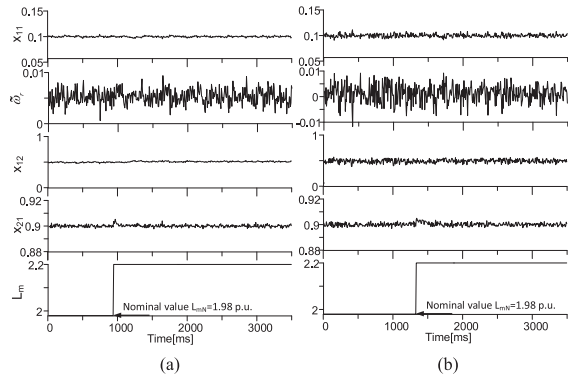

Fig. 7. Stationary state: the main, stator and rotor inductances are changed from 1.98 to 2.2 p.u., machine is loaded about 0.5 p.u., (a) backstepping-based speed observer and (b) STA-based speed observer.

A. Drive Starting, Speed Reversal, and Very Low Speed Reverse

The first scenario is presented in Fig. 4. The IM is starting up to 1.0 p.u. The STA introduces more oscillations to the state variables than the structure with the backstepping based observer

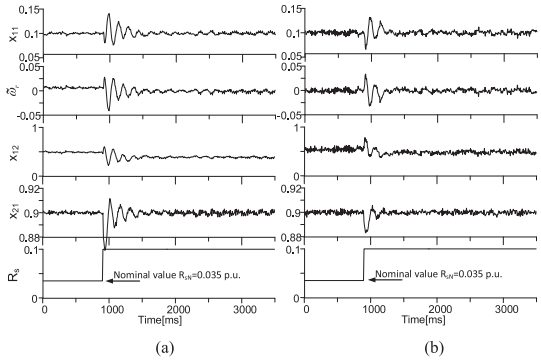

Fig. 8. Stationary state: the stator resistance is changed from 0.035 to 0.1 p.u. ($R_s = 2.85R_{sN}$), machine is loaded about 0.5 p.u. (a) backstepping-based speed observer and (b) STA-based speed observer.

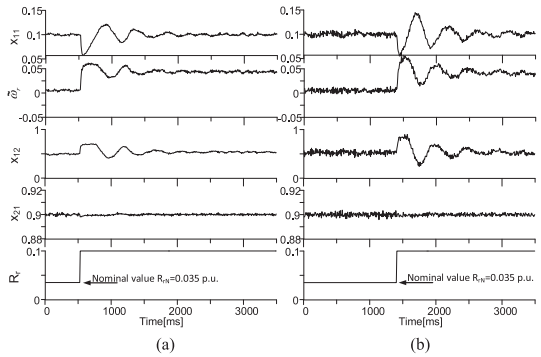

Fig. 9. Stationary state: the stator resistance is changed from 0.035 to 0.1 p.u. ($R_r = 2.85R_{rN}$), machine is loaded about 0.5 p.u., (a) backstepping-based speed observer and (b) STA-based speed observer.

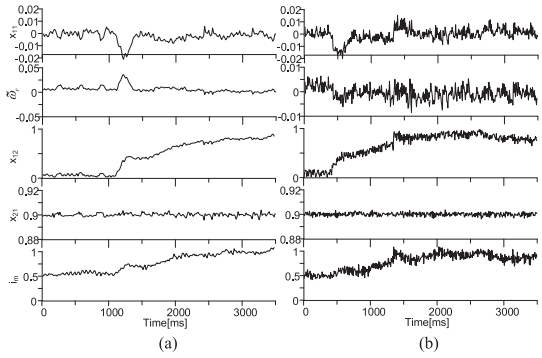

Fig. 10. Machine is loaded to 0.9 p.u. (after 1 s) in case of (a) backstepping-based speed observer and (b) STA-based speed observer.

what is shown in Fig. 4(b), however, the level of these oscillations is smaller than in the case of FOSM (for example [20]).

In Fig. 5, the IM is reversing from 0.95 to −0.95 p.u. In this case near to zero rotor speed, the square of rotor flux (x_{21}) variable has higher oscillations [see Fig. 5(a)] than in Fig. 5(b). Similarly, the variable x_{22} is more oscillated in Fig. 5(a) than in the case presented in Fig. 5(b). During the reverse, the estimated

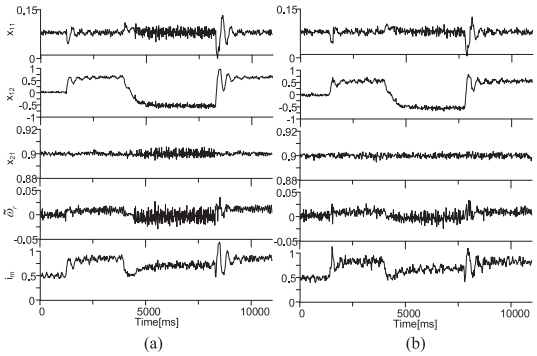

Fig. 11. Machine is loaded about +0.6 p.u. (after 1s – the IM works in the motor mode) and after 3.5 s IM is loaded −0.6 p.u. and after 8 s again +0.6 p.u. (IM works in regenerating mode) (a) backstepping-based speed observer and (b) STA-based speed observer.

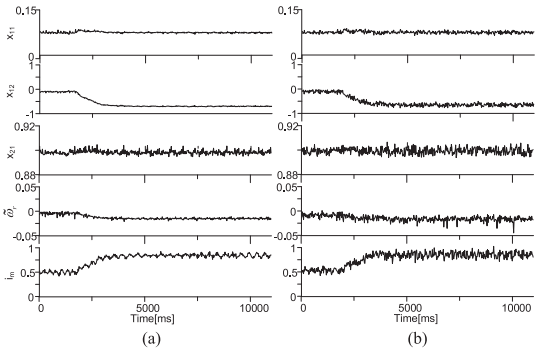

Fig. 12. After 1s IM machine is loaded about −0.6 p.u. (regenerating mode) for (a) backstepping-based speed observer structure and (b) STA-based speed observer.

rotor speed sticks to zero—it goes on only a few ms but it is visible in Fig. 5(a), however, in the waveforms of the presented variables from Fig. 5(b) this phenomena does not occur.

In Fig. 6, the IM very small speed reverse is presented (from 0.005 to −0.005—7.2 r/min). The very low speed test shows that speed observer structure which is based on STA approach is more robust than the backstepping one. For STA the rotor angular speed error is near to zero (for the backstepping the estimated speed error is about 0.02 p.u.). The sliding-mode properly excites the observer structure and it improves the observer properties.

B. Uncertenties of IM Parameters

In scenario 2, the nominal parameters of IM are detuned ($R_s \neq R_{sN}$, $R_r \neq R_{rN}$, $L_m \neq L_{mN}$). The main and the stator and rotor inductances are changed from (1.98 to 2.2 p.u. - $L_m = 1.1L_{mN}$), the load torque is 0.5 p.u., the rotor speed is 0.1 p.u. This case is shown in Fig. 7(a). The observer structure is not sensitive to changes of the IM inductances. Their influence on observer structure stability is negligible (for the inductance change up to 10% of nominal value and assumed working conditions).

In Fig. 8, the stator resistance R_s is changed $R_s = 2.85R_{sN}$. The estimated rotor speed error is near to zero in stationary state but the estimated electromagnetic toque value is changed. This

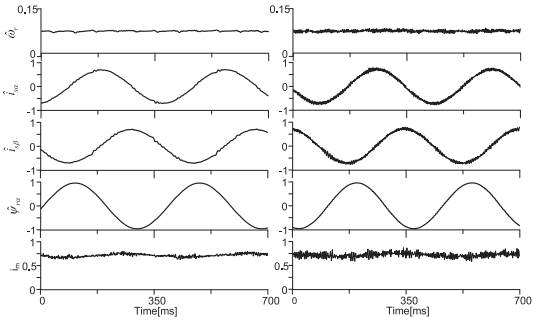

Fig. 13. Waveforms of reconstructed: rotor speed $\hat{\omega}_r$, stator current vector components $\hat{i}_{s\alpha}, \hat{i}_{s\beta}$, rotor flux vector component $\hat{\psi}_{r\alpha}$ and module of stator current vector i_m for (a) backstepping-based speed observer structure and (b) STA-based speed observer.

TABLE I
COMPARISON OF SELECTED PROPERTIES OF THREE STRUCTURES OF THE SPEED OBSERVERS (FOSM [20], PROPOSED STA AND BACKSTEPPING OBSERVER STRUCTURES)

Name	FOSM with backstepping [20]	STA structure	Proposed backstepping structure
Chattering	appears - the biggest	appears – but has smaller value than in FOSM	does no occur
Robustness in uncertainties	better than backstepping structure	Better than FOSM	the worst of all
Stable in zero speed	stable	stable	stable
Very low speed reverse	better than backstepping	better than FOSM	worse than STA and FOSM
Machine start-up/reverse	stable	stable	stable
Error of estimated rotor speed for different working points	comparable values	comparable values	comparable values
Medium and nominal speed with load torque injections	stable	stable	stable
Zero speed and load torque	sometimes it may not hold on the load torque but is stable	always hold on the load torque	always hold on the load torque
Regenerating mode and small speed	sometimes it may not hold on the load torque	better than FOSM	the same like STA

shows that the angle between the estimated rotor flux vector and stator current vector is different.

In Fig. 9, the rotor resistance R_r is changed $R_r = 2.85R_{rN}$. The change of rotor resistance has a huge impact on estimation quality. The rotor speed error is about 0.05 p.u. for the backstepping and STA. These tests show that the sensorless control system is stable, but the properties are not sufficient (during the rotor resistance is detuned especially).

C. Load Torque Injections for Low Rotor Speed

In the third experimental research scenario, the zero rotor speed was applied and almost nominal load torque was injected. This case is shown in Fig. 10. Both sensorless control system are robust on the load torque injections even if the zero speed is applied.

TABLE II
COMPUTING TIME OF THE SENSORLESS CONTROL SYSTEM WITH THE FOSM [20], AFO [31], [32], PROPOSED STA AND BACKSTEPPING

Name	FOSM [20]	STA structure	Proposed backstepping structure	AFO [31-32]
Computing time in [μs]	51	43	41	38.3

TABLE III
IM PARAMETERS AND REFERENCES UNIT

Symbol	Quantity	Values
R_{sN}	stator resistance	2.92 Ω/0.035 p.u.
R_{rN}	rotor resistance	3.36 Ω/0.032 p.u.
L_{mN}	magnetizing inductance	0.422 H/1.95 p.u.
L_s, L_r	stator and rotor inductance	0.439 H/2.04 p.u.
L_σ	leakage inductance	0.017 H/0.09 p.u.
P_n	nominal power	5.5 kW
I_n	nominal stator current (Y)	11 A
U_n	nominal stator voltage (Y)	400 V
n	nominal rotor speed	1430 rpm
f	nominal frequency	50 Hz
U_b=U_n	reference voltage	400 V
$I_b = I_n\sqrt{3}$	reference current	19 A
P_b	reference power	7.6 kW

In Fig. 11, the steps load torque injections are presented for the motor as well as in regenerating modes. After 1 s the load torque value was +0.6–0.7 p.u. and after 3.5 s the IM is loaded −0.6–0.7 p.u. In this case, IM works in regenerating mode—the reference rotor speed is +0.08 p.u. (comparable conditions as in [31] and [32]) and the reference load torque value is −0.6–0.7 p.u. The regenerating mode is a very difficult test for the sensorless control because the stator voltage vector has small value about 0.05–0.08 p.u. and the frequency of stator voltage is very small—these conditions are close to unobservable area of IM [17], [37]. The proposed sensorless control structure was stable for the presented in Fig. 11 working points. In case of STA speed observer [see Fig. 11(b)], the control system was more robust than the backstepping based—the square of rotor flux vector (x_{21}), x_{12} and x_{11} have a smaller level of oscillations in regenerating mode.

Fig. 12 presents the waveforms of multi-scalar variables, error of the estimated rotor speed $\hat{\omega}_r$ and the module of stator current vector i_m. The reference speed is 0.08 p.u. After 1 s the IM is loaded about –0.6 p.u., through what it works in the regenerating mode. In this working points the module of the stator current is about 0.8–0.9 p.u. and the estimated electromagnetic torque (x_{12}) near to 0.6–0.65 p.u. The error of estimated rotor speed is smaller than 0.015 p.u. for the backstepping observer structure but higher than for the STA structure (the average value of estimated speed error is smaller than 0.01 p.u.). It is results from the nature of sliding-mode approach and through what the STA observer structure is more robust than the backstepping one. Fig. 13 presents the waveforms of estimated rotor speed $\hat{\omega}_r$, stator current vector components $\hat{i}_{s\alpha}, \hat{i}_{s\beta}$, rotor flux vector component $\hat{\psi}_{r\alpha}$ and the module of stator current vector i_m during the IM machine works in the regenerating mode (the load torque value is about −0.5 p.u.).

The experimental results presented inthis section show that the both proposed observer structure are stable in the chosen working ranges and the STA is more robust than the

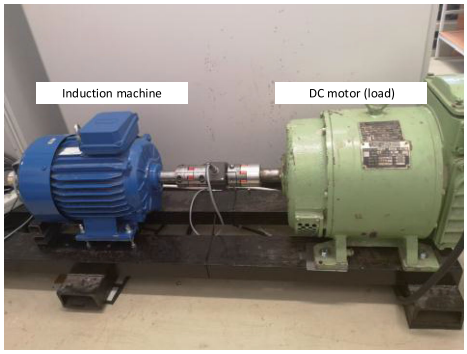

Fig. 14. Laboratory stand used in the experimental researches.

backstepping one, especially in the uncertainties of the IM parameters and during the regenerating mode and very low speed. In the case of STA structure the chattering in the presented state variables is visible. The analysis of experimental results shows that the observer system only with the backstepping continuous stabilizing functions has worse properties than a noncontinuous stabilizing control law. The STA structure is more robust in a very low speed range especially (<7 r/min), but in the waveforms of presented state variables the chattering effect is visible (higher oscillations)—the level of the chattering is very low but visible and almost inaudible while the electric drive is running. Introduced in (44) C_f parameter improves the properties of IM especially near to zero speed and during the regenerating mode.

In Table I, the three structure of the speed observers are compared. The first one is FOSM presented in [20] and proposed in Sections III and V backstepping-based structure and STA. Presented in Table I comparison is not accurate, but "roughly" represents the properties of the observer structures.

The computing times of the sensorless control system with selected speed observer structures: FOSM [20], AFO [31], [32], proposed STA and backstepping are given in Table II.

VII. Conclusion

This article presented two speed observer structures. The first one was based on a modified backstepping approach and the second one was based on sliding STA. The primary mathematical mode was extended to the integrator structures, therefore, the speed observer structures contained six differential equations. Taking into account the introduced $\vec{S}$ vector the value of estimated rotor speed results from the vector and scalar product.

The main contributions of this article were the speed observer structures which work stable under parameter uncertainties of IM as well as in the regenerating machine mode with low rotor speed. All assumptions was confirmed by the experimental results. The observer structure presented in this article will be further developed in the direction of chattering effect reduction and toward higher order sliding-mode solutions. Proposed observer structure was recommended to industrial applications, in which the measured and estimated electrical speed are necessary, for example in the electrical cars, trams, trains, or buses. In such applications stable observer-controller structure allows to failure-free electric drive system.

Appendix

The control system with the multiscalar variables is shown in Fig. 3. The multi-scalar variables were proposed in [33] and they are defined as follows:

$$x_{11} = \hat{\omega}_r \tag{54}$$

$$x_{12} = \hat{\psi}_{r\alpha}\hat{i}_{s\beta} - \hat{\psi}_{r\beta}\hat{i}_{s\alpha} \tag{55}$$

$$x_{21} = \hat{\psi}_{r\alpha}^2 + \hat{\psi}_{r\beta}^2 \tag{56}$$

$$x_{22} = \hat{\psi}_{r\alpha}\hat{i}_{s\alpha} + \hat{\psi}_{r\beta}\hat{i}_{s\beta} \tag{57}$$

where $\hat{\omega}_r$ is the estimated rotor speed value, $\hat{i}_{s\alpha}, \hat{i}_{s\beta}$ are the estimated stator current vector components and $\hat{\psi}_{r\alpha}, \hat{\psi}_{r\beta}$ are the estimated rotor flux vector components.

Using the mathematical model of IM and taking into account multiscalar transformation (54)–(57) the multiscalar model can be obtained [33].

The feedback linearizing controls (decoupling) are obtained, as follows:

$$u_1 = \frac{w_\sigma}{L_r}\left(m_1 + x_{11}\left(x_{22} + \frac{L_m}{w_\sigma}x_{21}\right)\right) \tag{58}$$

$$u_2 = \frac{w_\sigma}{L_r}\left(m_2 - x_{11}x_{22} - \frac{R_r L_m}{w_\sigma L_r}x_{21} - \frac{R_r L_m}{L_r}i_s^2\right) \tag{59}$$

where

$$w_\sigma = L_s L_r - L_m^2 \tag{60}$$

$$T_x = \frac{R_r L_s + R_s L_r}{w_\sigma} \tag{61}$$

$$i_s^2 = \hat{i}_{s\alpha}^2 + \hat{i}_{s\beta}^2 \tag{62}$$

where $m_{1,2}$ are new introduced control variables (treated as the PI controllers outputs presented in Fig. 3) and the multiscalar model of IM takes the following form:

$$\frac{dx_{11}}{d\tau} = \frac{L_m}{JL_r}x_{12} - \frac{1}{J}T_L \tag{63}$$

$$\frac{dx_{12}}{d\tau} = T_x\left(-x_{12} + m_1\right) \tag{64}$$

$$\frac{dx_{21}}{d\tau} = -2\frac{R_r}{L_r}x_{21} + 2\frac{R_r L_m}{L_r}x_{22} \tag{65}$$

$$\frac{dx_{22}}{d\tau} = T_x\left(-x_{22} + m_2\right). \tag{66}$$

The control variables of IM are determined

$$u_{s\alpha} = \frac{\hat{\psi}_{r\alpha}u_2 - \hat{\psi}_{r\beta}u_1}{x_{21}} \tag{67}$$

$$u_{s\beta} = \frac{\hat{\psi}_{r\alpha}u_1 + \hat{\psi}_{r\beta}u_2}{x_{21}} \tag{68}$$

where u_1 and u_2 were marked (in the multiscalar model) by

$$\begin{aligned} u_1 &= \hat{\psi}_{r\alpha}u_{s\beta} - \hat{\psi}_{r\beta}u_{s\alpha} \\ u_2 &= \hat{\psi}_{r\alpha}u_{s\alpha} + \hat{\psi}_{r\beta}u_{s\beta} \end{aligned}. \tag{69}$$

Fig. 14 presents the experimental stand with the two coupled machines (5.5 kW squirrel-cage IM and dc machine).

References

[1] P. Kakosimos, A. G. Sarigiannidis, M. Beniakar, A. Kladas, and Ch. Gerada, "Induction motors versus permanent-magnet actuators for aerospace applications," *IEEE Trans. Ind. Electron.*, vol. 61, no. 8, pp. 4315–4325, Aug. 2014. doi: 10.1109/TIE.2013.2274425.

[2] Z. Gao, L. Turner, R. S. Colby, and B. Leprettre, "A frequency demodulation approach to induction motor speed detection," *IEEE Trans. Ind. Appl.*, vol. 47, no. 4, pp. 1632–1642, Jul./Aug. 2011.

[3] Q. Tang, A. Shen, P. Luo, H. Shen, W. Li, and X. He, "IPMSMs sensorless MTPA control based on virtual Q-axis inductance by using virtual high frequency signal injection," *IEEE Trans. Ind. Electron.*, vol. 67, no. 1, pp. 136–146, Jan. 2020.

[4] B. Du, Z. Tianxu, S. Han, L. Song, and S. Cui, "Sensorless control strategy for IPMSM to reduce audible noise by variable frequency current injection," *IEEE Trans. Ind. Electron.*, vol. 67, no. 2, pp. 1149–1159, Feb. 2020.

[5] Q. Gao, G. Asher, and M. Sumner, "Sensorless position and speed control of induction motors using high-frequency injection and without offline precommissioning," *IEEE Trans. Ind. Electron.*, vol. 54, no. 5, pp. 2474–2481, Oct. 2007.

[6] D. Wang, L. Zhang, J. Zhang, X. Zhao, and X. Lin, "A hybrid speed sensorless control of induction machine based on adaptive flux observer and high-frequency signal injection method," in *Proc. IEEE 19th Work. Con. Mod. Power Elect.*, 2018, pp. 1–5.

[7] T. Berger, "On observers for nonlinear differential-algebraic systems," *IEEE Trans. Autom. Control*, vol. 64, no. 5, pp, 2150–2157, May 2019.

[8] J. You, W. Wu, and Y. Wang, "An adaptive luenberger observer for speed-sensorless estimation of induction machines," *in Proc. Ann. Amer. Control Conf.*, 2018, pp. 307–312.

[9] Z. Yin, G. Li, Y. Zhang, and J. Liu, "Symmetric-strong-tracking-extended-kalman-filter-based sensorless control of induction motor drives for modeling error reduction," *IEEE Trans. Ind. Informat.*, vol. 15, no. 2, pp. 650–662, Feb. 2019.

[10] M. Bouheraoua, J. Wang, and K. Atallah, "Rotor position estimation of a pseudo direct-drive PM machine using extended Kalman filter," *IEEE Trans. Ind. Appl.*, vol. 53, no. 2, pp. 1088–1095, Mar./Apr. 2017.

[11] W. Sun, K. Liu, D. Jiang, and R. Ou, "Zero synchronous speed stable operation strategy for speed sensorless induction motor drive with virtual voltage injection," in *Proc. IEEE Energy Convers. Congr. Expo.*, 2018, pp. 337–343, doi: 10.1109/ECCE.2018.8557756.

[12] A. N. Smith, S. M. Gadoue, and J. W. Finch, "Improved rotor flux estimation at low speeds for torque MRAS-based sensorless induction motor drives," *IEEE Trans. Energy Convers.*, vol. 31, no. 1, pp. 270–282, Mar. 2016.

[13] M. Morawiec, "Z type observer backstepping for induction machines," *IEEE Trans. Ind. Electron.*, vol. 62, no. 4, pp. 2090–2103, Apr. 2015.

[14] D. Karagiannis and V. Radisavljevic-Gajic, "A backstepping boundary observer for a simply supported beam," *IEEE Trans. Autom. Control*, vol. 64, no. 9, pp. 3809–3816, Sep. 2019, doi: 10.1109/TAC.2018.2884677.

[15] W. Sun, Y. Yu, G. Wang, B. Li, and D. Xu, "Design method of adaptive full order observer with or without estimated flux error in speed estimation algorithm," *IEEE Trans. Power Electron.*, vol. 31, no. 3, pp. 2609–2626, Mar. 2016.

[16] Y. B. Zbede, S. M. Gadoue, and D. J. Atkinson, "Model predictive MRAS estimator for sensorless induction motor drives," *IEEE Trans. Ind. Electron.*, vol. 63, no. 6, pp. 3511–3521, Jun. 2016.

[17] D. Traore, F. Plestan, A. Glumineau, and J. de Leon, "Sensorless induction motor: High-order sliding-mode controller and adaptive interconnected observer," *IEEE Trans. Ind. Electron.*, vol. 55, no. 11, pp. 3818–3827, Nov. 2008.

[18] M. A. Hamida, J. De Leon, A. Glumineau, and R. Boisliveau, "An adaptive interconnected observer for sensorless control of PM synchronous motors with online parameter identification," *IEEE Trans. Ind. Electron.*, vol. 60, no. 2, pp. 739–748, Feb. 2013.

[19] M. S. Zaky, M. K. Metwaly, H. Z. Azazi, and S. A. Deraz, "A new adaptive SMO for speed estimation of sensorless induction motor drives at zero and very low frequencies," *IEEE Trans. Ind. Electron.*, vol. 65, no. 9, pp. 6901–6911, Sep. 2018.

[20] M. Morawiec and A. Lewicki, "Application of sliding switching functions in backstepping based speed observer of induction machine," *IEEE Trans. Ind. Electron.*, vol. 67, no. 7, pp. 5843–5853.

[21] X. Zhang and Z. Li, "Sliding-mode observer-based mechanical parameter estimation for permanent magnet synchronous motor," *IEEE Trans. Power Electron.*, vol. 31, no. 8, Aug. 2016.

[22] L. Zhao, J. Huang, H. Liu, B. Li, and W. Kong, "Second-order sliding-mode observer with online parameter identification for sensorless induction motor drives," *IEEE Trans. Ind. Electron.*, vol. 61, no. 10, pp. 5280–5289, Oct. 2014, doi: 10.1109/TIE.2014.2301730.

[23] M. Ghanes and Z. Gang, "On sensorless induction motor drives: Sliding-mode observer and output feedback controller," *IEEE Trans. Ind. Electron.*, vol. 56, no. 9, pp. 3404–3413, Sep. 2009.

[24] M. Comanescu, "Design and implementation of a highly robust sensorless sliding mode observer for the flux magnitude of the induction motor," *IEEE Trans. Energy Convers.*, vol. 31, no. 2, pp. 649–657, Jun. 2016, doi: 10.1109/TEC.2016.2516951.

[25] A. Levant, "Robust exact differentiation via sliding mode technique," *Automatica*, vol. 34, no. 3, pp. 379–384, Mar. 1998.

[26] J. Davila, L. Fridman, and A. Levant, "Second-order sliding modes observer for mechanical systems," *IEEE Trans. Autom. Control*, vol. 50, no. 11, pp. 1785–1789, Dec. 2005.

[27] J. A. Moreno, *Lyapunov-Based Dsgn. of Homogen. High-Order Slid. Modes*. Cham, The Netherlands: Springer, 2018, pp. 3–38.

[28] J. Rivera Dominguez, C. Mora-Soto, S. Ortega-Cisneros, J. J. Raygoza Panduro, and A. V. Loukianov, "Copper and core loss minimization for induction motors using high-order sliding-mode control," *IEEE Trans. Ind. Electron.*, vol. 59, no. 7, pp. 2877–2889, Jul. 2012.

[29] M. Krsti´c, I. Kanellakopoulos, and P. Kokotovi´c, *Nonlinear and Adaptive Control Design.* New York, NY, USA: Wiley, 1995.

[30] A. Levant, "Sliding order and sliding accuracy in sliding mode control" *Int. J. Control*, vol. 58, no. 58, pp 1247–1263, 1993.

[31] M. Hinkkanen and J. Luomi, "Stabilization of regenerating-mode operation in sensorless induction motor drives by full-order flux observer design," *IEEE Trans. Ind. Electron.*, vol. 51, no. 6, pp. 1318–1328, Dec. 2004.

[32] Ch. Luo, B. Wang, Y. Yu, Ch. Chen, Z. Huo, and D. Xu, "Operating-point tracking method for sensorless induction motor stability enhancement in low-speed regenerating mode," *IEEE Trans. Ind. Electron.*, vol. 67, no. 5, pp. 3386–3397, May 2020.

[33] Z. Krzemiński, "Nonlinear control of induction motor," in *Proc. 10th IFAC World Congr.*, Munich, Germany, 1987, pp. 349–354.

[34] A. Levant, "Principles of 2-sliding Mode Design," *Automatica*, vol. 43, no. 4, pp. 576–586, Apr. 2007.

[35] M. Widmar, "Electric vehicle traction motors without rare earth magnets," *Sustain. Mater. Technol.*, vol. 3 pp. 7–13, 2015, doi: 10.1016/j.susmat.2015.02.001. ISSN 2214-9937.

[36] K. Wang, W. Yao, K. Lee, and Z. Lu, "Regenerating mode stability improvements for combined voltage and current mode flux observer in speed sensorless induction machine control," *IEEE Trans. Ind. Appl.*, vol. 50, no. 4, pp. 2564–2573, Jul./Aug. 2014.

[37] S. Ibarra-Rojas, J. Moreno, and G. Espinosa, "Global observability analysis of sensorless induction motor," *Automatica*, vol. 40, no. 6, pp. 1079–1085, 2004

Marcin Morawiec received the M.Sc. degree in electrical engineering from the Czestochowa University of Technology, Czestochowa, Poland, in 2003, and the Ph.D. and D.Sc. degrees in electrical engineering from the Gdansk University of Technology, Gdansk, Poland, in 2007 and 2017, respectively.

Since 2017, he has been an Associate Professor with the Department of Electric Drives and Energy Conversion with the Gdansk University of Technology. He has authored over 70 articles, two monographs, two chapters in books, one Polish patent, and five patent applications. His research interests include multiscalar models, nonlinear control of any electrical machines, sensorless control, nonlinear control, backstepping control, adaptive observer backstepping, and sliding mode control.

Arkadiusz Lewicki received the Ph.D. and D.Sc. degrees in electrical drives from the Faculty of Electrical Engineering, Gdansk University of Technology, Gdansk, Poland, in 2003 and 2013, respectively.

He is currently with the Institute of Automatic Control of Electric Drives, Gdansk University of Technology. His current research interests include microprocessor control of converters, multilevel converters, pulsewidth modulation techniques, and nonlinear control of drives.